Switching Control of Image-Based Visual Servoing With Laser Pointer in Robotic Manufacturing Systems

Wen-Fang Xie, *Member, IEEE*, Zheng Li, Xiao-Wei Tu, and Claude Perron

***Abstract*—In this paper, an Eye-in-Hand robotic system with laser pointer is developed to detect, grasp, and assemble a planar object on a main body in robotic manufacturing systems. This paper is focused on detecting the object and moving the end effector to a position where a pump can perfectly suck up the object. A switching control of image-based visual servoing (IBVS) is designed to control the pose of the end effector with respect to the stationary object so that the image features of the planar object observed by the camera converge to the target image features for the further assembly. A simple off-the-shelf laser pointer is adopted to realize the depth estimation for obtaining the image Jacobian matrices. By using a laser spot as an image feature and the separate degree-of-freedom method, the proposed switch-control algorithm decouples the rotational and translational motions of the camera to avoid the inherent drawbacks of traditional IBVS. The experiments on a robotic assembly system are given to verify the effectiveness of the proposed method.**

***Index Terms*—Control systems, laser pointer, robot vision systems, visual servoing.**

I. Introduction

TO REDUCE the labor cost and increase the throughput in the manufacturing industry, there is an increasing demand for automated robotic manufacturing systems such as robotic assembly, bin picking, drilling, and palletizing systems, which require accurate and fast robot positioning. The 3-D machine vision system is normally used in a robotic manufacturing system to compensate for the robotic positioning errors due to unforeseen work environment and randomly placed objects. The task of robot positioning using vision system is referred to as visual servoing, which aims at controlling the pose of the robot's end effector relative to a target object or a set of target features [1]–[4]. According to the features used as feedback in minimizing the positioning error, visual servoing is classified into three categories, position-based visual servoing (PBVS) [1], [5], [6], image-based visual servoing (IBVS) [7]–[9], [20], and hybrid visual servoing [19].

Since IBVS was introduced in 1980, it has attracted the attention of many researchers and has been tremendously developed in recent years. The method is based on the principle that when the image-feature error in 2-D image space is approaching zero, then the kinematical error in Cartesian space also approaches zero [1]. In IBVS, the error for the controller is defined directly with respect to the image-feature parameters [7]. Compared with PBVS, the advantages of IBVS are obvious. First, it is object model free and robust to camera modeling and hand–eye calibration errors [8]. Second, the image-feature point trajectories are controlled to move approximately along straight lines in the image plane. Hence, it is able to prevent the image features from leaving the field-of-view (FOV). However, the drawbacks of IBVS lie in the following aspects. Since the control law is merely designed in the image plane, the trajectory of the end effector in Cartesian space is not a straight line and even odd in some cases. In other words, in order to reduce the image-feature error to zero as soon as possible, unnecessary motions of the end effector are performed. Moreover, the system is stable only in a region around the desired position, and there may exist image singularities and image local minima [9], leading to IBVS failure. The choice of the visual features is a key point in solving the problem of image singularities. Lots of studies have been done to find out the decoupled visual features with respect to the 6 DOF of the robot. Such studies also ensure that the trajectory in Cartesian space is like a straight line [16], [18], [23], [24]. In [16], six image-moment features were selected to design a decoupled control scheme. In [18], Pages *et al.* derived the image Jacobian matrix related to a laser spot as an image feature. The global convergences of the control law had been shown with a constant interaction matrix. However, the method needed the information of the planar object and only fit for the situation where the camera was located near the desired position. Another approach using a laser pointer in visual servoing was presented in [24]; Krupa *et al.* developed a vision system with stationary camera, which retrieved and positioned surgical instruments for operation. A laser pointer was used to project laser spot on the organ surface to control the depth. However, the servoing was only carried out in 3 DOF, and the camera was motionless. Therefore, the system could not provide much flexibility in visual servoing in large-scale environment.

Manuscript received February 14, 2008; revised July 14, 2008. First published August 19, 2008; current version published January 30, 2009. This work was supported in part by the Institute for Aerospace Research, National Research Council Canada (NRC) and in part by the Natural Sciences and Engineering Research Council of Canada (NSERC) under a Discovery Research Grant.

W.-F. Xie and Z. Li are with the Department of Mechanical and Industrial Engineering, Concordia University, Montreal, QC H3G 1M8, Canada (e-mail: wfxie@encs.concordia.ca; richard_lizheng@hotmail.com).

X.-W. Tu and C. Perron are with the Aerospace Manufacturing Technology Centre, National Research Council Canada, Montreal, QC H3T 2B2, Canada (e-mail: Xiao-Wei.Tu@cnrc-nrc.gc.ca; Claude.Perron@cnrc-nrc.gc.ca).

Color versions of one or more of the figures in this paper are available online at http://ieeexplore.ieee.org.

Digital Object Identifier 10.1109/TIE.2008.2003217

Hashimoto and Noritsugu [10] introduced a method to solve the image local minima. The main idea was to define a potential function and to minimize it while controlling the robot. If the potential had local minima, the algorithm generated an artificial potential and then controlled the camera based on the artificial one. In [11], stereo-based visual servoing was proposed to solve the depth-estimation problem and calculate an exact image Jacobian matrix. However, this kind of algorithm increased the computational cost. Mahony *et al.* [21] introduced a method of choosing other types of image features instead of points for IBVS and focusing on the depth axis control. Oh and Allen [22] presented a partitioning degree-of-freedom (DOF) method for IBVS which used a 3-DOF robot with a 2-DOF pan tilt unit. The experimental results of tracking people were given. In [25], another partitioned approach to visual-servoing control was introduced, which decoupled the z-axis rotational and translational components of the control from the remaining DOF.

To overcome the aforementioned shortcomings of IBVS, some new approaches that integrate PBVS and IBVS methods have been developed [15], [19]. The main idea is to use a hybrid of Cartesian and image-space sensory feedback signals to control both Cartesian and image trajectories simultaneously. One example of such hybrid approach is 2.5D visual servoing [19], which was based on the estimation of the partial camera displacement. Recently, a hybrid motion-control and planning strategies for image-constraint avoidance was presented in [12] and [13]. This motion-control part included a local switching control between the IBVS and PBVS for avoiding image singularity and image local minima. In addition, the planning strategy was composed of an artificial hybrid trajectory planner.

Inspired by the hybrid motion-control and planning strategies, we proposed a new switch-control approach to IBVS to overcome the shortcomings of IBVS. First, a laser pointer is adopted to realize online depth estimation to obtain image Jacobian matrix. Second, we added a laser-point image feature to the chosen image features of the object. Based on the new image-feature set, we can detect the object in the workspace even when the features of object are in FOV partially. Hence, the available workspace is virtually enlarged to some extent. Furthermore, a set of imaginary target features is introduced so that a decoupled control scheme for IBVS can be designed. Third, we separated 3-DOF rotational motion from the translational motion to solve some image-singularity problem such as 180° rotation around the optical axis [9] and image local minima in IBVS. This decoupled control strategy can make visual-servoing system work over a large region around the desired position.

This switch-control approach to IBVS with laser pointer is applied to a robotic assembly system. The system is composed of a 6-DOF robot, a camera mounted on the robot end effector, a simple off-the-shelf laser pointer rigidly linked to the camera, and a vacuum pump for the object grasping. The whole algorithm consists of three steps. First, the laser spot is driven onto a planar object. Since the laser pointer is mounted on the robot end effector, 3-DOF rotational motion of end effector can drive the object image features close to a set of imaginary image features so that the laser spot is projected on the object. Next, the image features of the object and laser spot are used to obtain the image Jacobian matrix, which is primarily used for controlling the end-effector translational motion with respect to the object. Finally, a constant image Jacobian at the desired camera configuration for IBVS is used to adjust the fine alignment so that the feature errors can reach to the image global minimum. The successful application of the proposed algorithm to an experimental robotic assembly system demonstrates the effectiveness of the proposed method.

This paper is organized as follows. In Section II, the problem statement of visual servoing is introduced. A novel approach to switching control of IBVS with laser pointer is presented in Section III. In Section IV, several experimental results are given to show the effectiveness of the proposed method. The concluding remarks are given in Section V.

II. Problem Statement

In this paper, we focus on an automated robotic assembly system which uses Eye-in-Hand architecture to perform visual servoing. In this system, the assembly task is to move the robot end effector together with a tool, such as a gripper or a vacuum pump, to approach a part with unknown pose and, then, to grasp and assemble it to a main body fast and smoothly. Such an assembly task is a typical visual-servoing control problem. Hence, IBVS is an appropriate method to achieve the task, since all control input is computed in an image space without using the pose information.

Let $\dot{r} = [{}^{C}v_{C} \quad {}^{C}\omega_{C}]^{\mathrm{T}} = [v_x \quad v_y \quad v_z \quad \omega_x \quad \omega_y \quad \omega_z]^{\mathrm{T}}$ be a velocity screw of the camera. Define $f_i = [x_i \quad y_i]^{\mathrm{T}}$, $i = 1, 2, \ldots, n$, as the image features and $\dot{f}_i = [\dot{x}_i \quad \dot{y}_i]^{\mathrm{T}}$ as the corresponding image-feature velocity. Denote the desired image feature as $f_{di} = [x_{di} \quad y_{di}]^{\mathrm{T}}$ and $f_d = [f_{d1} \quad f_{d2} \quad \cdots \quad f_{dn}]^{\mathrm{T}}$ which are obtained by using a teaching-by-showing approach. In this paper, the teaching procedures are as follows: 1) Move the robot end effector to a position where the pump can perfectly suck up the object; 2) move the robot in end-effector frame to a new position where the whole object is in the FOV, and record this moving value as the constant transformation; and 3) take an image as the target image for visual servoing. The four coplanar corners of the object are chosen as the target image features, and the laser spot $f_d^l = [x_d^l \quad y_d^l]^{\mathrm{T}}$ is also selected as a target image feature in some cases.

Assume that the effective sizes of a pixel (s_x, s_y) are constant to simplify the visual-servoing computation without loss of generality. The transformation between $[x_i \quad y_i]^{\mathrm{T}}$ and the pixel indexes $[u \quad v]^{\mathrm{T}}$ depends only on camera intrinsic parameters.

In order to design the feedback control for robot based on the velocity of the feature points, we have the following relationship between the motion of image features and the physical motion of the camera:

$$\dot{f} = \mathbf{J}_{\mathrm{img}}(f, Z)\dot{r} \tag{1}$$

where

$$\mathbf{J}_{\mathrm{img}}(f, Z) = \begin{bmatrix} \mathbf{J}_{\mathrm{img}}(f_1, Z_1) \\ \vdots \\ \mathbf{J}_{\mathrm{img}}(f_n, Z_n) \end{bmatrix} \tag{2}$$

is the image Jacobian matrix, $Z = [Z_1, \ldots, Z_n]^{\mathrm{T}}$ is the depth of each feature point, and $f = [f_1, \ldots, f_n]^{\mathrm{T}}$ is the image-feature vector containing n features.

For each feature point (x_i, y_i), the image Jacobian matrix is represented as follows:

$$\mathbf{J}_{\mathrm{img}}(f_i, Z_i) = \begin{bmatrix} \frac{\lambda}{Z_i} & 0 & -\frac{x_i}{Z_i} & -\frac{x_i y_i}{\lambda} & \frac{\lambda^2 + x_i^2}{\lambda} & -y_i \\ 0 & \frac{\lambda}{Z_i} & -\frac{y_i}{Z_i} & \frac{-\lambda^2 - y_i^2}{\lambda} & \frac{x_i y_i}{\lambda} & x_i \end{bmatrix} \tag{3}$$

where λ is the known focal length of the camera.

Equation (1) can be written as

$$\dot{r} = \mathbf{J}^{+}_{\mathrm{img}}(f, Z)\dot{f} \tag{4}$$

where $\mathbf{J}^{+}_{\mathrm{img}}(f, Z)$ is the pseudoinverse of the image Jacobian. If the error function is defined as $e(f) = f - f_d$ and we impose $\dot{e}(f) = -Ke(f)$, a simple proportional control law is given by

$$\dot{r} = -K\mathbf{J}^{+}_{\mathrm{img}}(f, Z)e(f) \tag{5}$$

where $\dot{r}$ is the camera velocity sent to the robot controller, K is the proportional gain which tunes the exponential convergence rate of f toward f_d.

It is assumed that the optical axis of the camera is coincident with the Z-axis of the end effector. The motion of camera can be related to robot joint rates through the normal robot Jacobian and a fixed transformation between the motion of the camera and the end effector. When the image error function $e(f)$ tends to zero, the kinematical error must also approach zero. However, an inappropriate choice of $\mathbf{J}^{+}_{\mathrm{img}}(f, Z)$ may lead the system close to, or even cause, a singularity of the Jacobian matrix, which may result in potential servoing failure [19].

The objective of IBVS in this paper is to control the end effector to approach an unknown object so that the image error function $e(f)$ approaches zero while the trajectory in the Cartesian space is kept as short as possible. Meanwhile, the system should be designed with low cost, and the visual-servoing algorithm is developed with low computational load for real-time robot control.

III. IBVS With Laser System

In this section, a new approach to switching control of IBVS with laser pointer is presented to accomplish the aforementioned visual-servoing tasks. This approach is designed to overcome the drawbacks of IBVS by installing an off-the-shelf laser pointer on the end effector for estimating the depth of the image features and separating the visual-servoing procedures into several control stages.

A. Robotic Eye-in-Hand System

The designed robotic Eye-in-Hand system configuration is shown in Fig. 1, which is composed of a 6-DOF robot, a camera mounted on the robot end effector, a laser pointer rigidly linked to the camera, and a vacuum pump for grasping object. In Fig. 1, $\mathbf{H}$ denotes the transformation between two reference frames.

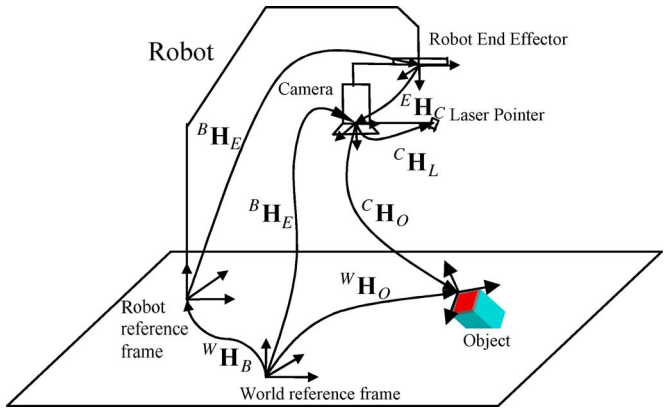

Fig. 1. Robotic Eye-in-Hand system configuration.

In traditional IBVS, since the control law is only designed in the image plane, unnecessary motions of the end effector are performed. In order to obtain the image Jacobian $\mathbf{J}_{\mathrm{img}}(f, Z)$ which is a function of features and depths of object, depth estimation is needed for each feature point. A low-cost laser pointer is thus adopted and installed on the end effector to measure the distance from the camera to the target for depth estimation. Through the laser triangulation method, the depth estimation can be achieved in a very short time. Moreover, the laser spot can be chosen as an image feature that eases the image processing with low computational load for visual servoing.

B. Online Depth Estimation

In (3), $\mathbf{J}_{\mathrm{img}}(f, Z)$ is a function of features and their depths. Although one of the solutions to IBVS is to choose the target image features and their depths for a constant image Jacobian, it is proved to be stable only in a neighborhood of the desired position. Another solution is to estimate the depth of every feature point online. In this paper, a simple laser-pointer-based triangulation method is applied to estimate the depth online.

Assume that the laser beam is lying in the same plane with the camera optical axis. We use a camera-center frame $\{c\}$ with ${}^{C}z$ parallel to the optical axis. In this configuration, no matter how camera is moving, the trajectory of the laser spot in the image is a straight line passing the principal point. If we consider the laser pointer as a camera and the laser beam is its optical axis, the straight line in the image is an epipolar line of the imaginary stereo configuration.

As shown in Fig. 2, d denotes the horizontal distance between the laser beam and the optical axis of lens of the camera, and α is the angle between the laser beam and the horizontal line. Both of them are fixed and known when the laser pointer is installed. Point P is the intersecting point of the laser beam and the object surface. A function of depth Z_p with respect to pixel indexes (u, v) [17] is derived by applying the trigonometry. The depth Z_p calculated by (6) can be used to approximate the depth of each feature point in the planar object surface under the assumption that the size of object is small enough

$$Z_p = \frac{d \sin \alpha}{\cos(\alpha - \beta)} \tag{6}$$

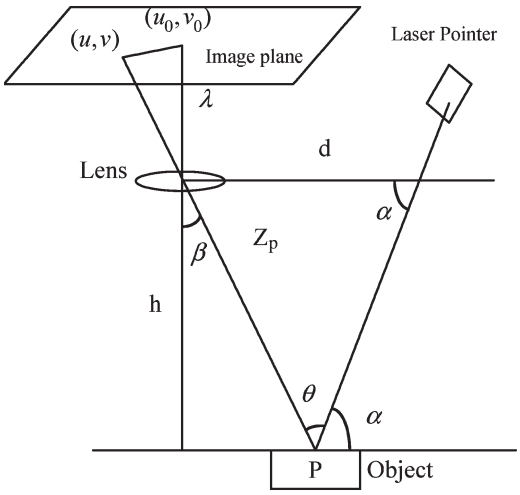

Fig. 2. Calculation of the depth of a point by using triangulation.

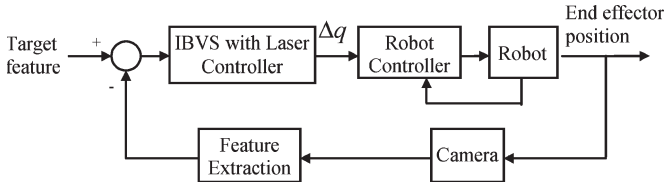

Fig. 3. Block diagram of IBVS with laser control system.

where β is the triangle inside the camera.

Remark: It is noted that (6) is only valid when the camera and the laser are planar. In the robotic assembly system, the laser pointer is rigidly linked to the camera in a frame which is attached to the end effector of the robot. Inside the frame, the laser pointer is installed in a way that the laser line and object camera projections are coplanar. The possible generalization of this calibration phase to the case on noncoplanar laser and camera is under investigation.

C. Switching Control of IBVS With Laser Pointer

The proposed algorithm is divided into three control stages which are as follows: 1) driving the laser spot on the object, 2) combining IBVS with laser spot for translational moving, and 3) adjusting the fine alignment. The block diagram of the switching control system of IBVS with laser pointer is shown in Fig. 3. The object is assumed to be stationary with respect to robot reference frame.

Stage 1—Driving the Laser Spot on the Object: To project the laser spot on the object, two kinds of situations need to be considered. One is that all features are in the FOV (Stage 1.A), and the other is that certain features are missing in the FOV (Stage 1.B). Both of them are discussed as follows in detail.

Stage 1.A—All Features in the FOV: When all image features are in the FOV, the control task is to drive the center of gravity of the object together with the image features of object near the current laser spot and the created imaginary image features by using 3-DOF camera motion. Equation (1) can be decomposed into translational and rotational component parts as shown as follows:

$$\dot{f} = \begin{bmatrix} \mathbf{J}^t_{\text{img}}(f, Z) & \mathbf{J}^r_{\text{img}}(f) \end{bmatrix} \begin{bmatrix} {}^C v_C \\ {}^C \omega_C \end{bmatrix} \tag{7}$$

where $\mathbf{J}^t_{\text{img}}(f, Z)$ and $\mathbf{J}^r_{\text{img}}(f)$ are stacked by $\mathbf{J}^t_{\text{img}}(f_i, Z_i)$ and $\mathbf{J}^r_{\text{img}}(f_i)$, respectively, given by

$$\mathbf{J}^t_{\text{img}}(f_i, Z_i) = \begin{bmatrix} \frac{\lambda}{Z_i} & 0 & -\frac{x_i}{Z_i} \\ 0 & \frac{\lambda}{Z_i} & -\frac{y_i}{Z_i} \end{bmatrix} \tag{8}$$

$$\mathbf{J}^r_{\text{img}}(f_i) = \begin{bmatrix} -\frac{x_i y_i}{\lambda} & \frac{\lambda^2 + x_i^2}{\lambda} & -y_i \\ \frac{-\lambda^2 - y_i^2}{\lambda} & \frac{x_i y_i}{\lambda} & x_i \end{bmatrix}. \tag{9}$$

It is noted that $\mathbf{J}^t_{\text{img}}$ is related to both features and their depths, and $\mathbf{J}^r_{\text{img}}$ is only a function of the image features. Since the laser pointer is mounted on the robot end effector, it is possible to control it by performing 3-DOF rotational motion. It is known that 2 DOF of rotational motion can drive a laser pointer to project its dot image on the target. In this paper, the reason of using 3 DOF instead of 2 DOF is that the rotation along the camera Z-axis can be used to solve some image-singularity problems such as 180° rotation around the optical axis, which is well-known case causing visual-servoing failure as presented by Chaumette [9]. To avoid this particular case, a set of imaginary target features are designed. Based on the target image features including the desired object features f_d and the laser spot f^l_d, a new imaginary image can be designed, which is shown in Fig. 4. Let the distance between the target position of laser spot and the current laser spot be $d_l = \|f^l_d - f^l\|$. The imaginary object features f_{iof} are formed by shifting all target object features f_{di} by units d_l and adding the current laser spot f^l

$$f_{\text{iof}} = [\, f_{dl} - d_1 \quad f_{d2} - d_l \quad \cdots \quad f_{dn} - d_l \quad f^l \,]^{\text{T}}. \tag{10}$$

It is assumed that the height of the object is relatively small. Hence, there is no big discrepancy of the laser spot in the image plane when the laser spot moves from the workspace platform to the surface of object.

The center of gravity of object image features is served as an extra image feature which is defined as $f_{\text{cg}} = [(x_1 + \cdots + x_n)/n, (y_1 + \cdots + y_n)/n]^{\text{T}}$ in the image plane. The control goal is to minimize the error norm between the image features $f_{s1A} = [f_1 \quad f_2 \cdots f_n \quad f_{\text{cg}}]^{\text{T}}$ and the imaginary features, as presented as follows:

$$\min \{\|f_{s1A} - f_{\text{iof}}\|\}. \tag{11}$$

From (7), the relationship between the motion of the image features and the rotational DOF of camera ${}^C\omega_C$ is represented as

$$\dot{f}_{s1A} = \begin{bmatrix} \mathbf{J}^t_{\text{img}}(f_{s1A}, Z_{s1A}) & \mathbf{J}^r_{\text{img}}(f_{s1A}) \end{bmatrix} \begin{bmatrix} {}^C v_C \\ {}^C \omega_C \end{bmatrix} \tag{12}$$

where $Z_{s1A} = [Z_1 \quad Z_2 \cdots Z_n \quad Z^l]^{\text{T}}$.

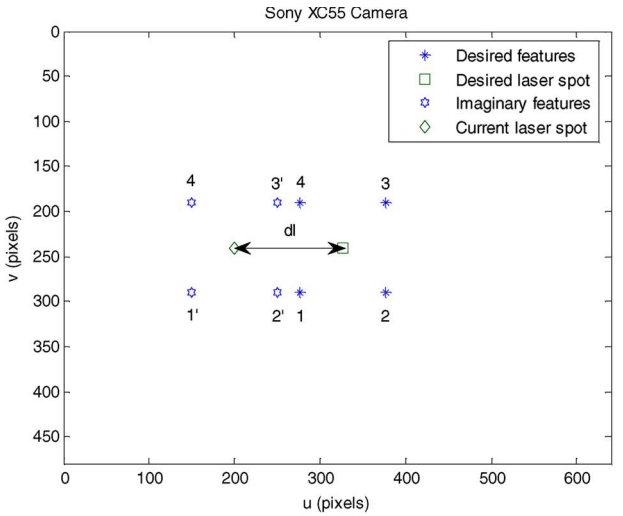

(a)

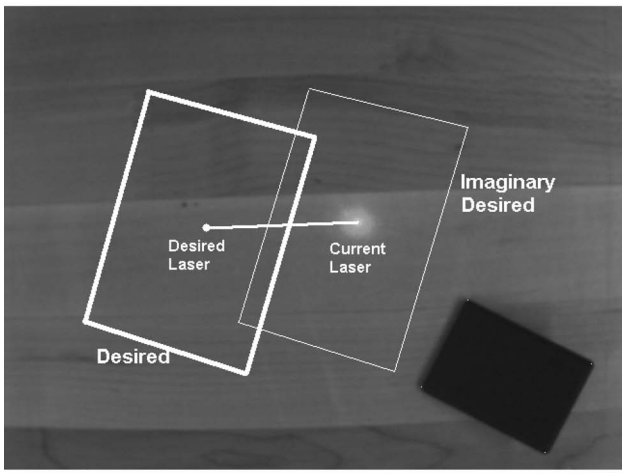

(b)

Fig. 4. Example of creating imaginary features. (a) In 2-D image space. (b) In 3-D Cartesian space.

The earlier equation can be written as

$$^{C}\omega_{C} = \mathbf{J}^{r}_{\text{img}}{}^{+}(f_{S1A})\left[\dot{f}_{s1A} - \mathbf{J}^{t}_{\text{img}}(f_{s1A}, Z_{s1A})^{C}v_{C}\right]. \quad (13)$$

We set the translational DOF of camera motion as zero ($^{C}v_{C} = 0$), and the following equation is obtained:

$$^{C}\omega_{C} \cong \mathbf{J}^{r}_{\text{img}}{}^{+}(f_{s1A})\left[\dot{f}_{s1A}\right]. \quad (14)$$

Let the feature error defined as $e_{\text{iof}} = f_{s1A} - f_{\text{iof}}$. By imposing $\dot{e}_{\text{iof}} = -K_l e_{\text{iof}}$, one can design the proportional control law given by

$$u_{s1A} = {}^{C}\omega_{C} = -K_l \mathbf{J}^{r}_{\text{img}}{}^{+}(f)e_{\text{iof}} \quad (15)$$

where $^{C}\omega_{C}$ is the camera angular velocity sent to the robot controller and K_l is the proportional gain.

Since we deliberately turn off the translational motion of camera, (14) relating the image velocity to 3-DOF camera rotational motion is approximately held. The proportional controller (15) cannot make the feature-error e_{iof} approach zero exponentially. However, the current control task is only to drive the laser spot on the object and rotate the camera to make the image features of the object approach the imaginary features. The further tuning of visual servoing will be carried out in the next stages. Hence, we adopt the switching rule to switch the controller to the second stage.

The switching rule is described as follows: When the error norm falls below a predetermined threshold value, the controller will switch from current stage to the second stage. The switching condition is given by

$$\|f_{\text{iof}} - f_{s1A}\| \le f_{s1A\_0} \quad (16)$$

where f_{s1A_0} is the predetermined feature-error threshold value.

Therefore, the controller (15) is expressed as follows:

$$u_{s1A} = {}^{C}\omega_{C} = \begin{cases} -K_l \mathbf{J}^{r}_{\text{img}}{}^{+}(f)e_{\text{iof}}, & \|f_{\text{iof}} - f_{s1A}\| > f_{s1A\_0} \\ u_{s2}, & \text{otherwise.} \end{cases} \quad (17)$$

Notice that the function of this control law not only drives the laser spot on the object but also solves the image-singularity problem. As mentioned in [9], a pure rotation of 180° around the optical axis leads to image singularity and causes a pure backward translational camera motion along the optical axis. In the proposed algorithm, the 3-DOF rotation of the camera is mainly executed in the first stage of control, and the translational movement of camera is primarily executed in the second stage of control. Hence, the backward translational camera motion is avoided.

Stage 1.B—Features Partially Seen in the FOV: When only partial object is in the FOV, some features are not available. In order to obtain all the features, we propose a strategy to control 2-DOF rotational motion of camera to project the laser spot on the centroid of the object in image plane until the whole object appears in the FOV. Hence, the motion of the laser image feature $f^{l} = [x^{l} \quad y^{l}]^{\mathrm{T}}$ is related to the camera motion as

$$\dot{f}^{l} = \mathbf{J}^{r}_{\text{img}XY}(f^{l})\dot{r}_{xy} + \mathbf{J}_{\text{img\_cz}}(f^{l})\dot{r}^{\mathrm{T}}_{cz} \quad (18)$$

where $\dot{r}_{xy} = [\omega_x, \omega_y]^{\mathrm{T}}$ represents 2-DOF rotational motion of camera, $\dot{r}_{cz} = [v_x \quad v_y \quad v_z \quad \omega_z]^{\mathrm{T}}$ is the rest of camera velocity screw, the image Jacobian matrices $\mathbf{J}^{r}_{\text{img}XY}(f^{l})$ and $\mathbf{J}_{\text{img\_cz}}(f^{l})$ are defined, respectively, as

$$\mathbf{J}^{r}_{\text{img}XY}(f^{l}) = \begin{bmatrix} -\frac{x^{l}y^{l}}{\lambda} & \frac{\lambda^{2}+x^{l2}}{\lambda} \\ \frac{-\lambda^{2}-y^{l2}}{\lambda} & \frac{x^{l}y^{l}}{\lambda} \end{bmatrix}$$

$$\mathbf{J}_{\text{img\_cz}}(f^{l}, Z^{l}) = \begin{bmatrix} \frac{\lambda}{Z^{l}} & 0 & -\frac{x^{l}}{Z^{l}} & -y^{l} \\ 0 & \frac{\lambda}{Z^{l}} & -\frac{y^{l}}{Z^{l}} & x^{l} \end{bmatrix}. \quad (19)$$

Equation (18) can be written as

$$\dot{r}_{xy} = \mathbf{J}^{r}_{\text{img}XY}{}^{+}(f^{l})\left[\dot{f}^{l} - \mathbf{J}_{\text{img\_cz}}(f^{l}, Z^{l})\dot{r}^{\mathrm{T}}_{cz}\right] \quad (20)$$

where $\mathbf{J}^{r}_{\text{img}XY}{}^{+}(f^{l})$ is the pseudoinverse of image Jacobian matrix $\mathbf{J}^{r}_{\text{img}XY}(f^{l})$.

As aforementioned, 2 DOF of rotational motion $\dot{r}_{xy} = [\omega_x \quad \omega_y]^{\mathrm{T}}$ allows the laser pointer to project its dot image

close to the desired target. Thus, the other elements of the camera velocity screw $\dot{r}_{cz} = [v_x \quad v_y \quad v_z \quad \omega_z]^{\mathrm{T}}$ are set to zero. Equation (20) becomes

$$\dot{r}_{xy} \cong \mathbf{J}^{r}_{\mathrm{img}XY}{}^{+}(f^l)\dot{f}^l. \tag{21}$$

The centroid of the partial object in the image is used as the desired laser image feature for the laser spot. To attain such centroid, one generally calculates the first-order moments of the partial object image. Let R represents the region of the partial object in a binary image $I(k, j)$, which can be obtained by using fixed-level threshold. For a digital image, the moments of the region R are defined as

$$m_{kj} = \sum_{(x,y)\in R} x^k y^j, \qquad k \geq 0,\ j \geq 0 \tag{22}$$

where (x, y) represent the row and column of a pixel in the region R, respectively. According to the definition of moment, we have the area of the region R and the centroid of R as

$$A_R = m_{00} \tag{23}$$

$$f_c = \begin{bmatrix} f_{xc} \\ f_{yc} \end{bmatrix} = \begin{bmatrix} \frac{m_{10}}{m_{00}} \\ \frac{m_{10}}{m_{00}} \end{bmatrix} \tag{24}$$

where f_c is the centroid of the partial object in the image.

Define the image-feature error between the laser image feature and the centroid of partial object image feature as $e^l_c = [f^l - f_c]$. The proportional control law for 2 DOF of rotational motion is designed by imposing $\dot{e}^l_c = -K_{l2}e^l_c$

$$u_{s1B} = \dot{r}_{xy} = \begin{cases} -K_{l2}\mathbf{J}^{r+}_{\mathrm{img}XY}(f^l)e^l_c, & \|f^l - f_c\| > f_{s1B\_0} \\ u_{s1A}, & \text{otherwise} \end{cases} \tag{25}$$

where K_{l2} is the proportional gain and f_{s1B_0} is the predetermined feature-error threshold value.

When the image-feature error e^l_c enters into the range $\|f^l - f_c\| \leq f_{s1B\_0}$, the laser spot is projected close to the planar object. In this paper, the end effector is assumed to be posed above the planar object, and the FOV is relatively large as compared with the image of the object. Hence, all the feature points enter into FOV when the laser spot is close to the desired laser image ($\|f^l - f_c\| \leq f_{s1B\_0}$). Once all the feature points are obtained, the control law is switched to u_{s1A} in Stage 1.A.

Stage 2—Translational Moving of Camera: The key problem in switch control of Stage 2 is how to obtain the image Jacobian matrix of relating the motion of image features plus laser spot to the translational motion of camera. According to the derivation of traditional image Jacobian matrix, the target is supposed to be stationary. Hence, the laser spot on the object can be considered as a stationary point adapting to image Jacobian matrix of traditional IBVS. Based on earlier scheme, the algorithm is presented in detail as follows.

Let $f_{s2} = [f_1 \cdots f_n f^l]^{\mathrm{T}}$ represents n image features plus the laser image feature $f^l = [x^l \quad y^l]^{\mathrm{T}}$. It is assumed that the object is small as compared with the workplace. Hence, the depth of the laser image close to the centroid of the object can be treated as a good approximation to the depth of all features. The modified relationship between the motion of the image features and the motion of camera is given by

$$\dot{f}_{s2} = \mathbf{J}_{\mathrm{img}}(f_{s2}, Z^l)\dot{r} \tag{26}$$

where $\mathbf{J}_{\mathrm{img}}(f_{s2}, Z^l)$ can also be decomposed into translational and rotational component parts, as shown as follows:

$$\mathbf{J}_{\mathrm{img}}(f_{s2}, Z^l) = \begin{bmatrix} \mathbf{J}^t_{\mathrm{img}}(f_{s2}, Z^l) & \mathbf{J}^r_{\mathrm{img}}(f_{s2}) \end{bmatrix} \tag{27}$$

where the two components are formed as

$$\mathbf{J}^t_{\mathrm{img}}(f_{s2}, Z^l) = \begin{bmatrix} \mathbf{J}^t_{\mathrm{img}}(f_1, Z^l) \\ \vdots \\ \mathbf{J}^t_{\mathrm{img}}(f_n, Z^l) \\ \mathbf{J}^t_{\mathrm{img}}(f^l, Z^l) \end{bmatrix}$$

$$\mathbf{J}^r_{\mathrm{img}}(f_{s2}) = \begin{bmatrix} \mathbf{J}^r_{\mathrm{img}}(f_1) \\ \vdots \\ \mathbf{J}^r_{\mathrm{img}}(f_n) \\ \mathbf{J}^r_{\mathrm{img}}(f^l) \end{bmatrix}. \tag{28}$$

Equation (26) can be written as

$$\begin{aligned} \dot{f}_{s2} &= \begin{bmatrix} \mathbf{J}^t_{\mathrm{img}}(f_{s2}, Z^l) & \mathbf{J}^r_{\mathrm{img}}(f_{s2}) \end{bmatrix} \begin{bmatrix} {}^C v_C \\ {}^C\omega_C \end{bmatrix} \\ &= \mathbf{J}^t_{\mathrm{img}}(f_{s2}, Z^l){}^C v_C + \mathbf{J}^r_{\mathrm{img}}(f_{s2}){}^C\omega_C. \end{aligned} \tag{29}$$

Moreover, the translational motion of the camera is derived as

$${}^C v_C = \mathbf{J}^t_{\mathrm{img}}{}^{+}(f_{s2}, Z^l)\left[\dot{f}_{s2} - \mathbf{J}^r_{\mathrm{img}}(f_{s2}){}^C\omega_C\right]. \tag{30}$$

Set the rotational motion of the camera to zero. The earlier equation is rewritten as

$${}^C v_C \cong \mathbf{J}^t_{\mathrm{img}}{}^{+}(f_{s2}, Z^l)\dot{f}_{s2}. \tag{31}$$

The control objective is to move the image features of object plus the laser spot image close to the target image features by using the translational motion of the camera. The target image features include four coplanar corner points of object image plus the desired laser spot f^l_d defined as $f_{s2\_D} = [f_{d1} \quad f_{d2} \cdots f_{dn} \quad f^l_d]^{\mathrm{T}}$. The error between them is defined as follows: $e_{s2} = f_{s2} - f_{s2\_D}$.

The translational motion of the camera is designed by imposing $\dot{e}_{s2} = -K_{s2}e_{s2}$

$$\begin{aligned} u_{s2} &= {}^C v_C \\ &= \begin{cases} -K_{s2}\mathbf{J}^t_{\mathrm{img}}{}^{+}(f_{s2}, Z^l)e_{s2}, & \|f_{s2} - f_{s2\_D}\| > f_{s2\_0} \\ u_{s3}, & \text{otherwise} \end{cases} \end{aligned} \tag{32}$$

where K_{s2} is the proportional gain and f_{s2_0} is the predetermined feature-error threshold value.

The switching rule is described as follows: if the image-feature-error norm between the current image features and the desired image features falls below a threshold f_{s2_0}, the IBVS

with laser pointer switches from the current stage to the third stage u_{s3}

$$\|f_{s2} - f_{s2\_D}\| \leq f_{s2\_0}. \tag{33}$$

Since the translational motion of camera is approximately derived as (31), the proportional controller (32) cannot drive the image feature e_{s2} to approach zero exponentially. However, the translational motion brings the image of object in the vicinity of target image features. A switching rule is thus set to switch from the current stage to the next one for the fine tuning of visual servoing. The threshold f_{s2_0} is directly related to the depth and affects the stability of the controller. Thus, the selection of this threshold is crucial, and it is normally set as relatively small pixels to maintain the stability of the system.

Stage 3—Adjusting the Fine Alignments: After applying the switching controllers in Stages 1 and 2, one can control the end effector to the neighbor of the target image features. It has been presented in [9] that the constant image Jacobian at the desired camera configuration can be used to reach the image global minimum. Hence, a constant image Jacobian matrix can be used in IBVS to adjust the fine alignment of end effector so that the pump can perfectly suck up the object. In this stage, the laser image feature is not considered as an image feature, and the traditional IBVS with constant image Jacobian of target image features is applied.

Since the image features are close to their desired position in the image plane, as shown in (33), the depths of the points of image features are approximate to the desired ones (essentially planar object). The target features and their corresponding depths are applied to the traditional IBVS with constant image Jacobian matrix shown as

$$\mathbf{J}_{\text{img}}(f_{id}, Z_{id}) = \begin{bmatrix} \frac{\lambda}{Z_{id}} & 0 & -\frac{x_{id}}{Z_{id}} & -\frac{x_{id}y_{id}}{\lambda} & \frac{\lambda^2+x_{id}^2}{\lambda} & -y_{id} \\ 0 & \frac{\lambda}{Z_{id}} & -\frac{y_{id}}{Z_{id}} & \frac{-\lambda^2-y_{id}^2}{\lambda} & \frac{x_{id}y_{id}}{\lambda} & x_{id} \end{bmatrix} \tag{34}$$

where f_{id} and Z_{id} are target features and their corresponding depths, respectively.

The control goal of this stage is to control the pose of the end effector so that the image-feature error between the current image features $f = [f_1 \ \dots \ f_n]^{\mathrm{T}}$ and the target image features $f_d = [f_{d1} \ f_{d2} \ \dots \ f_{dn}]^{\mathrm{T}}$ reaches the global minimum. The condition can be described as follows: If the feature-error norm falls below a predetermined threshold, the whole IBVS with laser pointer will stop. The condition is presented as

$$\|f_d - f\| \leq f_{s3\_0} \tag{35}$$

where f_{s3_0} is a predetermined threshold value, $f = [f_1 \ \dots \ f_n]^{\mathrm{T}}$ is the image features, and $f_d = [f_{d1} \ f_{d2} \ \dots \ f_{dn}]^{\mathrm{T}}$ is the desired feature.

The proportional controller is designed as

$$u_{s3} = \begin{bmatrix} {}^{C}v_C \\ {}^{C}\omega_C \end{bmatrix} = \begin{cases} -\mathbf{J}_{\text{img}}^{+}(f_d, Z_d)(f - f_d), & \|f_d - f\| > f_{S3\_0} \\ \text{Stop Servoing} - \text{Start grasping}, & \text{otherwise} \end{cases} \tag{36}$$

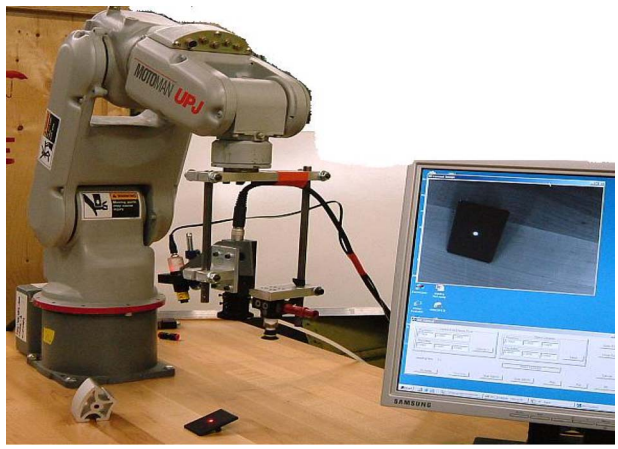

Fig. 5. Robotic assembly system setup and components to be assembled.

where K_{s3} is the proportional gain and $Z_d = [Z_{1d} \ \dots \ Z_{nd}]^{\mathrm{T}}$ is the depth vector of each target feature point.

The threshold f_{S3_0} directly affects the accuracy of the robot end-effector pose with respect to the object. The bigger the value of threshold is chosen, the less accurate pose will be achieved. However, the positioning process time is reduced.

It is noticed that the proposed IBVS algorithm is derived from traditional IBVS. Therefore, it inherits the advantages of IBVS, which does not need object model and is robust to the camera calibration and hand–eye calibration error. In addition, by using a laser pointer and the separate DOF method, the proposed switch algorithm decouples the rotational and translational motion controls of the robotic end effector to overcome the inherent drawbacks of traditional IBVS such as image singularities and the image local minima.

IV. Experimental Results

The proposed IBVS with laser pointer has been tested on a robotic assembly system including an industrial robot Motoman UPJ with JRC controller, a laser pointer, and a PC-based vision system including Matrox frame grabber and a Sony XC55 camera mounted on the robot. The robotic assembly system setup for testing IBVS with laser pointer is shown in Fig. 5

To verify the effectiveness of the proposed method, a plastic object shown in Fig. 5 is chosen to be assembled in a metallic part. The four coplanar corners of the surface are selected as the target features. One of the advantages of the JRC controller in UPJ robot is that it accepts the position and orientation values and calculates the joint angle by itself, which eliminates the robot kinematical modeling error. However, the drawback of the JRC controller is that it cannot be used for real-time control. In other words, when the designed controller generates a new position or orientation value and sends it to the JRC controller, it will not respond it until the previous position is reached in each iteration. With this limitation of hardware, we have to divide the calculated value into a serial of small increment by a constant factor in each step and also increase the sampling time. In the experiment, we chose constant factor as 50, and the sampling time as 2 s.

The desired pose ${}^{E}\mathbf{H}_O$ is set as [36 −66 123 0 0 13.7] (millimeters, degrees) for teaching procedure. The predetermined

TABLE I
GOOD AND BAD CALIBRATION VALUES OF SYSTEM PARAMETERS

Parameters	Good calibration values	Bad calibration values
Principal point (pixel)	[326 228]	[384 288]
Focal length (mm)	6.02	7.2
Effective size (mm)	0.0074×0.0074	0.0074×0.0074
${}^{C}\mathbf{H}_{L}$		
$[X\ Y\ Z\ \varphi\ \theta\ \psi]$ (mm, deg) measured by hand	[8 0 0 0 -18 0]	[6 0 0 0 -14 0]
${}^{E}\mathbf{H}_{C}$		
$[X\ Y\ Z\ \varphi\ \theta\ \psi]$ (mm, deg) calculated by calibration	[-7 5 189 -2 0 -179]	[-20 20 210 5 5 180]

threshold f_{s1A_0} in (16) is set as ten pixels, and f_{s1B_0} in (25) is set as ten pixels. The f_{s2_0} in (32) is tuned as ten pixels, which is approximately 28 mm in the experimental setup. f_{s3_0} in (35) is set as three pixels. All the proportional gains of control law are set as one. When the condition of feature-error norm falling below three pixels is met, the end effector is brought to the desired pose with respect to the plastic object. It should be noted that no matter where the object is located in the work-place, the desired pose of end effector with respect to the object is exactly the same. For any object position, there exists a fixed transformation between camera and end-effector frame with this desired pose. Before the visual servoing starts, we need to teach the robot this fixed pose once. Therefore, commanding the robot end effector to move the predefined transformation vector in end-effector frame perfectly lets the vacuum pump suck up the object. The assembled components shown in Fig. 5 demonstrate the accuracy of the proposed method.

A. With Good Calibration Value

The proposed algorithm is tested with good calibration values (Table I). The parameters d and α for the fixed laser–camera configuration are adjusted to 8 mm and 72° individually. The sequential pictures of successful assembly process are shown in Fig. 6. The image trajectory obtained from the experiment is shown in Fig. 7(a). The rectangular with white edges represents the initial position, and the black object shows the desired position. The object is posed manually with randomized initial position.

B. With Bad Calibration Value

To test the robustness of the IBVS with laser pointer, camera calibration error is also added to intrinsic parameters with 20% deviation as shown in Table I. The good and bad calibration values of transformation among camera reference, laser-pointer, and robot end-effector frames are also shown in Table I. The object position is the same as that of the experiment with good calibration value, and the image trajectory resulted from experiment is shown in Fig. 7(b).

Although the image trajectory shown in Fig. 7(b) is distorted as compared with the trajectory shown in Fig. 7(a), the image features still converge to the desired position, and the assembly task is also successfully accomplished. Hence, the proposed algorithm is very robust to the camera calibration and hand–eye calibration error on the order of 20% deviation from nominal values.

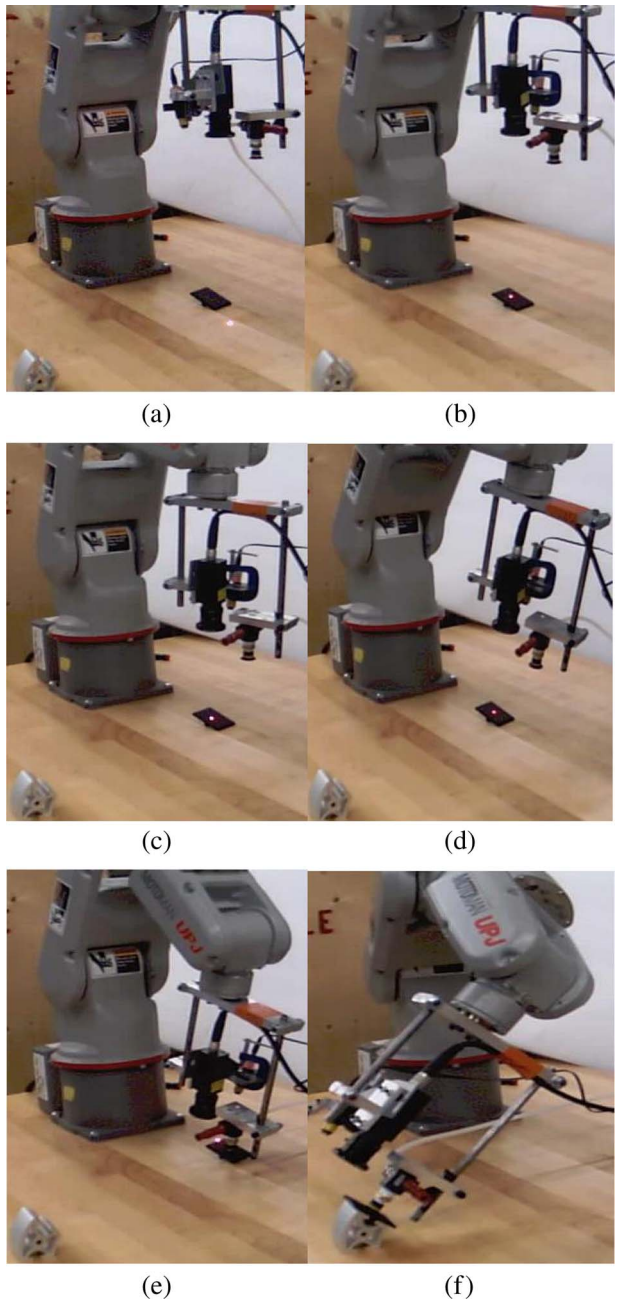

Fig. 6. Assembly sequence. (a) Initial position. (b) End of stage 1. (c) End of stage 2. (d) End of stage 3 (ready to pick up the object). (e) Suck up the object. (f) Assembly.

In order to test the depth-estimation convergence, the experiments on the depth estimation are carried out under the conditions with good and bad calibration values. The experimental results are shown in Fig. 8. Both results show that the estimated depths converge to the real distance, and thus, the depth-estimation convergences are experimentally proved.

V. CONCLUSION

In this paper, a new approach to IBVS with laser pointer was developed. The laser pointer was adopted, and the triangular

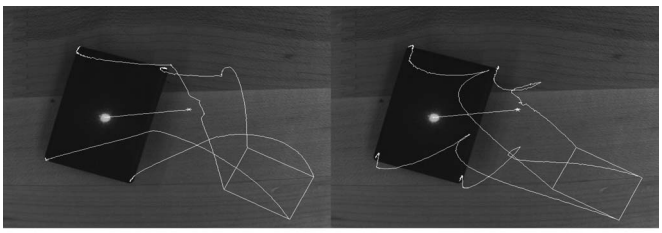

Fig. 7. Image trajectory. (a) With good calibration value. (b) With bad calibration value.

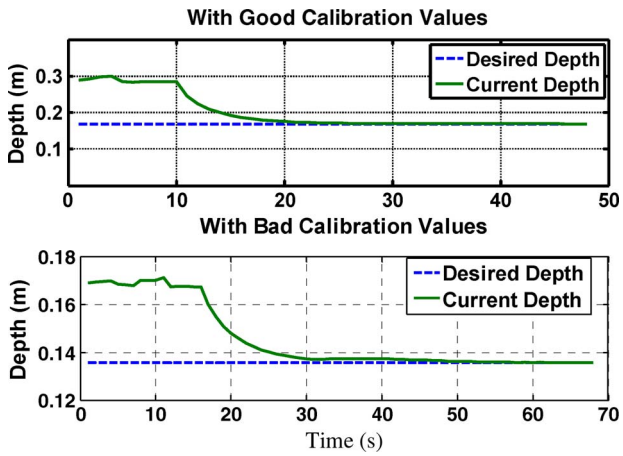

Fig. 8. Experimental results of depth estimation.

method was used to estimate the depth between the camera and the object. The switch control of IBVS with laser pointer is decomposed into three stages to accomplish visual-servoing tasks under various circumstances. The algorithm has been successfully applied in an experimental robotic assembly system. The experimental results verify the effectiveness of the proposed method and also validate the feasibility of applying the proposed method to industrial manufacturing systems. Future work includes testing the proposed method on a robot manipulator supporting real-time control and conducting analytical convergence analysis of switch-control algorithm.

REFERENCES

[1] S. Hutchinson, G. D. Hager, and P. I. Corke, "A tutorial on visual servo control," *IEEE Trans. Robot. Autom.*, vol. 12, no. 5, pp. 651–670, Oct. 1996.
[2] P. I. Corke, *Visual Control of Robots: High Performance Visual Servoing*. New York: Res. Stud. Press, 1996.
[3] Z. Li, W. F. Xie, and N. Aouf, "A neural network based hand–eye calibration approach in robotic manufacturing systems," in *Proc. CSME*, Calgary, AB, Canada, May 21–24, 2006. CD-ROM.
[4] N. Aouf, H. Rajabi, N. Rajabi, H. Alanbari, and C. Perron, "Visual object tracking by a camera mounted on a 6DOF industrial robot," in *Proc. IEEE Conf. Robot., Autom. Mechatronics*, Dec. 2004, vol. 1, pp. 213–218.
[5] D. F. DeMenthon and L. S. Davis, "Model-based object pose in 25 lines of code," *Int. J. Comput. Vis.*, vol. 15, no. 1/2, pp. 123–141, Jun. 1995.
[6] W. J. Wilson, C. C. W. Hulls, and G. S. Bell, "Relative end-effector control using Cartesian position-based visual servoing," *IEEE Trans. Robot. Autom.*, vol. 12, no. 5, pp. 684–696, Oct. 1996.
[7] L. E. Weiss, A. C. Sanderson, and C. P. Neuman, "Dynamic sensor-based control of robots with visual feedback," *IEEE J. Robot. Autom.*, vol. RA-3, no. 5, pp. 404–417, Oct. 1987.
[8] B. Espiau, "Effect of camera calibration errors on visual servoing in robotics," in *Proc. 3rd Int. Symp. Exp. Robot. III*, 1993, vol. 200, pp. 182–192.
[9] F. Chaumette, "Potential problems of stability and convergence in image based and position-based visual servoing," in *The Confluence of Vision and Control*, vol. 237, D. Kriegman, G. D. Hager, and A. Morse, Eds. Berlin, Germany: Springer-Verlag, 1998, pp. 66–78.
[10] K. Hashimoto and T. Noritsugu, "Potential problems and switching control for visual servoing," in *Proc. IEEE/RSJ Int. Conf. Intell. Robots Syst.*, Oct. 2000, vol. 1, pp. 423–428.
[11] H. Kase, N. Maru, A. Nishikawa, S. Yamada, and F. Miyazaki, "Visual servoing of the manipulator using the stereo vision," in *Proc. IEEE IECON*, 1993, vol. 3, pp. 1791–1796.
[12] L. Deng, F. Janabi-Sharifi, and W. J. Wilson, "Hybrid motion control and planning strategies for visual servoing," *IEEE Trans. Ind. Electron.*, vol. 52, no. 4, pp. 1024–1040, Aug. 2005.
[13] L. Deng, W. J. Wilson, and F. Janabi-Sharifi, "Dynamic performance of the position-based visual servoing method in the Cartesian and image spaces," in *Proc. IEEE/RSJ Int. Conf. Intell. Robots Syst.*, 2003, vol. 1, pp. 510–515.
[14] G. Chesi, K. Hashimoto, D. Prattichizzo, and A. Vicino, "Keeping features in the field of view in eye-in-hand visual servoing: A switching approach," *IEEE Trans. Robot.*, vol. 20, no. 5, pp. 908–913, Oct. 2004.
[15] N. R. Gans and S. A. Hutchinson, "An experimental study of hybrid switched system approaches to visual servoing," in *Proc. IEEE ICRA*, Sep. 2003, vol. 3, pp. 3061–3068.
[16] O. Tahri and F. Chaumette, "Point-based and region-based image moments for visual servoing of planar objects," *IEEE Trans. Robot.*, vol. 21, no. 6, pp. 1116–1127, Dec. 2005.
[17] E. Trucco and A. Verri, *Introductory Techniques for 3-D Computer Vision*. Englewood Cliffs, NJ: Prentice–Hall, 1998.
[18] J. Pages, C. Collewet, F. Chaumette, and J. Salvi, "Optimizing plane-to-plane positioning tasks by image-based visual servoing and structured light," *IEEE Trans. Robot.*, vol. 22, no. 5, pp. 1000–1010, Oct. 2006.
[19] E. Malis, F. Chaumette, and S. Boudet, "2-1/2-D visual servoing," *IEEE Trans. Robot. Autom.*, vol. 15, no. 2, pp. 238–250, Apr. 1999.
[20] J. P. Wang and H. Cho, "Micropeg and hole alignment using image moments based visual servoing method," *IEEE Trans. Ind. Electron.*, vol. 55, no. 3, pp. 1286–1294, Mar. 2008.
[21] R. Mahony, P. Corke, and F. Chaumette, "Choice of image features for depth-axis control in image based visual servo control," in *Proc. IEEE/RSJ Int. Conf. Intell. Robots Syst.*, 2002, vol. 1, pp. 390–395.
[22] P. Y. Oh and P. K. Allen, "Visual servoing by partitioning degrees of freedom," *IEEE Trans. Robot. Autom.*, vol. 17, no. 1, pp. 1–17, Feb. 2001.
[23] F. Janabi-Sharifi and M. Ficocelli, "Formulation of radiometric feasibility measures for feature selection and planning in visual servoing," *IEEE Trans. Syst., Man, Cybern. B, Cybern.*, vol. 34, no. 2, pp. 978–987, Apr. 2004.
[24] A. Krupa, J. Gangloff, C. Doignon, M. Mathelin, G. Morel, J. Leroy, L. Soler, and J. Marescaux, "Autonomous 3-D positioning of surgical instruments in robotized laparoscopic surgery using visual servoing," *IEEE Trans. Robot. Autom.*, vol. 19, no. 5, pp. 842–853, Oct. 2003.
[25] P. I. Corke and S. A. Hutchinson, "A new partitioned approach to image-based visual servo control," *IEEE Trans. Robot. Autom.*, vol. 17, no. 4, pp. 507–515, Aug. 2001.
[26] P. I. Corke, "A robotics toolbox for MATLAB," *IEEE Robot. Autom. Mag.*, vol. 3, no. 1, pp. 24–32, Mar. 1996.

Wen-Fang Xie (M'04) received the M.S. degree from Beijing University of Aeronautics and Astronautics, Beijing, China, in 1991, and the Ph.D. degree from The Hong Kong Polytechnic University, Kowloon, Hong Kong, in 1999.

She was an Industrial Research Fellowship holder of the Natural Sciences and Engineering Research Council of Canada, Ottawa, ON, Canada. She was a Senior Research Engineer with InCoreTec, Inc., St. John's, NL, Canada. She is currently an Associate Professor with the Department of Mechanical and Industrial Engineering, Concordia University, Montreal, QC, Canada. Her research interests include nonlinear control in mechatronics, artificial intelligent control, advanced process control and system identification, and visual servoing.

Zheng Li received the B.Eng. degree in electrical engineering from Harbin Institute of Technology, Harbin, China, in 1999, and the M.A.Sc. degree in mechanical engineering from Concordia University, Montreal, QC, Canada, in 2007.

During his M.A.Sc. studies, he also performed two years of joint research work with the Aerospace Manufacturing Technology Centre, National Research Council Canada, Ottawa, ON, Canada. He is currently with the Department of Mechanical and Industrial Engineering, Concordia University. His main research interests are in the area of visual servoing, machine vision, and motion control.

Xiao-Wei Tu received the Ph.D. degree in computer vision and image processing from Compiègne University of Technology, Compiègne, France, in 1987.

From 1988 to 1997, he was a Professor and then a Research Scientist in real-time vision system design, mobile robots, and pattern-recognition fields with the French National Research Center. From 1998 to early 2006, he was with the Industrial Research Center of Quebec, Canada, where he was a Research and Development Scientist and Engineer working in the field of robotic vision and industrial inspection projects. Since February 2006, he has been with the Aerospace Manufacturing Technology Centre, National Research Council Canada, Ottawa, ON, Canada. He is currently involved in projects of visual servoing for robots, surface inspection, and integration of automation systems in aerospace industries.

Claude Perron received the M.S. degree from the Ecole Polytechnique, Paris, France.

After working in several academic and industrial institutions, he joined the National Research Council (NRC) Institute for Aerospace Research in 2002 and created the Automation Robotics in Intelligent Manufacturing Group, Aerospace Manufacturing Technologies Center (AMTC), NRC, Montreal, QC, Canada. His research interests include aeroelasticity loads, automation, dynamics, and robotics.